MPMI Vol. X, No. X, XXXX, pp. X–X. https://doi.org/10.1094/MPMI-04-20-0081-R

Insights into Metabolic Changes Caused by the *Trichoderma virens*–Maize Root Interaction

Rabea Schweiger,[1] Fabiola Padilla-Arizmendi,[2] Guillermo Nogueira-López,[2] Michael Rostás,[2,3] Robert Lawry,[2] Chris Brown,[4] John Hampton,[2] Johanna M. Steyaert,[5] Caroline Müller,[1,†] and Artemio Mendoza-Mendoza[2,†]

[1] Department of Chemical Ecology, Bielefeld University, Universitätsstr. 25, 33615 Bielefeld, Germany
[2] Bio-Protection Research Centre, Lincoln University, Lincoln 7647, Canterbury, New Zealand
[3] Agricultural Entomology, Department of Crop Sciences, University of Göttingen, Grisebachstr. 6, 37077 Göttingen, Germany
[4] Department of Biochemistry, University of Otago, Dunedin 9054, New Zealand
[5] Lincoln Agritech Ltd., PO Box 69133, Lincoln, Christchurch 7460, New Zealand

Accepted 6 November 2020.

The interactions of crops with root-colonizing endophytic microorganisms are highly relevant to agriculture, because endophytes can modify plant resistance to pests and increase crop yields. We investigated the interactions between the host plant *Zea mays* and the endophytic fungus *Trichoderma virens* at 5 days postinoculation grown in a hydroponic system. Wild-type *T. virens* and two knockout mutants, with deletion of the genes *tv2og1* or *vir4* involved in specialized metabolism, were analyzed. Root colonization by the fungal mutants was lower than that by the wild type. All fungal genotypes suppressed root biomass. Metabolic fingerprinting of roots, mycelia, and fungal culture supernatants was performed using ultrahigh performance liquid chromatography coupled to diode array detection and quadrupole time-of-flight tandem mass spectrometry. The metabolic composition of *T. virens*-colonized roots differed profoundly from that of noncolonized roots, with the effects depending on the fungal genotype. In particular, the concentrations of several metabolites derived from the shikimate pathway, including an amino acid and several flavonoids, were modulated. The expression levels of some genes coding for enzymes involved in these pathways were affected if roots were colonized by the Δ*vir4* genotype of *T. virens*. Furthermore, mycelia and fungal culture supernatants of the different *T. virens* genotypes showed distinct metabolomes. Our study highlights the fact that colonization by endophytic *T. virens* leads to far-reaching metabolic changes, partly related to two fungal genes. Both metabolites produced by the fungus and plant metabolites modulated by the interaction probably contribute to these metabolic patterns. The metabolic changes in plant tissues may be interlinked with systemic endophyte effects often observed in later plant developmental stages.

Keywords: benzoxazinoids, endophytes, flavonoids, fungus–plant interactions, genomics, metabolomics, plant antifungal responses, plant–fungus symbiosis, plant–microbe interaction, roots, specialized (secondary) metabolism, secretion, *Trichoderma*

The growth, development, and health of plants are influenced by complex microbial communities living on and in the plants (Simon et al. 2019). In particular, the rhizosphere—the close zone between roots and soil—harbors a vast array of microorganisms. Communication between these microorganisms and roots is mediated by various metabolites (i.e., low molecular mass compounds) and proteins (Mhlongo et al. 2018; Morath et al. 2012). The ascomycetous fungi of the genus *Trichoderma* display an outstanding range of lifestyles, including free-living species in the rhizosphere as well as species that colonize plant roots (Brotman et al. 2013). The resulting endophyte–plant interactions are often beneficial for plants, because *Trichoderma* spp. can promote plant growth (Guzmán-Guzmán et al. 2019) and control plant pathogens through the production of toxins, hydrolytic enzymes, and volatile organic compounds (Cruz-Magalhães et al. 2019; Zeilinger et al. 2016). Therefore, they are frequently used as biofertilizers and for the biological control of soilborne fungal pathogens in the cultivation of crops such as maize (family Poaceae) (Druzhinina et al. 2011; Guzmán-Guzmán et al. 2019). However, despite widespread application and considerable research on *Trichoderma*–plant relationships, we lack a deeper understanding of the processes that regulate these symbioses.

Several "omics" technologies have been applied to study *Trichoderma*–plant interactions. Transcriptome analyses revealed that the gene expression of both the plant and its symbiont are differentially regulated upon root colonization (De Palma et al. 2019; Morán-Diez et al. 2015; Wang et al. 2020). Likewise, plant and fungal proteins are modulated during the establishment of the interaction (Lamdan et al. 2015; Marra et al. 2006;

R. Schweiger, F. Padilla-Arizmendi, and G. Nogueira-López contributed equally to this work.

†Corresponding authors: C. Müller; caroline.mueller@uni-bielefeld.de; and A. Mendoza-Mendoza; artemio.mendoza@lincoln.ac.nz

Funding: Support was provided by Deutsche Forschungsgemeinschaft grant INST 215/485-1 to C. Müller, Tertiary Education Commission Bio-Protection Research Centre grants to A. Mendoza-Mendoza, M. Rostás, F. Padilla-Arizmendi, and G. Nogueira-López, Consejo Nacional de Ciencia y Tecnología grant to G. Nogueira-López for his studies at Lincoln University, Royal Society Marsden grant LIU1001 to A. Mendoza-Mendoza and C. Brown, and Ministry of Business, Innovation & Employment grant MBIE LVLX1702 to J. M. Steyaert.

*The *e*-Xtra logo stands for "electronic extra" and indicates that a supplementary figure and supplementary table are published online.

The author(s) declare no conflict of interest.

Nogueira-Lopez et al. 2018). Often, the metabolome offers the most functional information (Fiehn et al. 2000). Metabolomics is increasingly being applied to characterize plant responses to environmental changes and to unravel underlying mechanisms. Indeed, metabolomics approaches are very useful to investigate plant metabolic responses to abiotic stresses and to uncover metabolic changes when plants interact with other plants, herbivores, or microbes (Peters et al. 2018; Schweiger et al. 2014b; Vaughan et al. 2018). Whereas shifts in plant metabolomes triggered by plant antagonists are well described, the use of metabolomics to unravel plant–mutualist interactions has just started to emerge. For instance, beneficial endophytic N_2-fixing bacteria were shown to affect the root metabolome of their host (Agtuca et al. 2020). Likewise, metabolomics approaches revealed pronounced modulations of primary and specialized metabolites in local (root) and systemic (leaf) tissues in response to root colonization with arbuscular mycorrhizal fungi (AMF) (Andrade et al. 2013; Schweiger and Müller 2015). Root colonization with *Trichoderma* spp. affects the concentrations of soluble sugars, amino acids, phenolic compounds, citrate cycle intermediates, and polyamines in leaves of different plant species (Brotman et al. 2012; Vinci et al. 2018; Yedidia et al. 2003). However, little is known about intra- and extracellular metabolic patterns of the fungi and metabolic responses in plant seedlings to the plant–fungus interaction.

Trichoderma spp. also induce systemic resistance in tissues far from the colonization site (Shoresh et al. 2010). For example, tomato (family Solanaceae) inoculated with *Trichoderma harzianum* T22 accumulated isoprenoids in leaves and showed an increased resistance against aphids (Coppola et al. 2019). Similarly, *T. velutinum* altered the concentrations of several primary and specialized metabolites in leaves of bean (family Fabaceae) (Mayo-Prieto et al. 2019). *T. harzianum* T-78 is also known to induce tomato resistance to the root knot nematode *Meloidogyne incognita* by shifting from salicylic acid- to jasmonic acid-based defenses (Martínez-Medina et al. 2017). However, the specific metabolic processes activated in maize roots during *Trichoderma*–plant interactions are mostly unexplored.

The use of *Trichoderma* mutants with deletions in genes associated with the symbiosis may deepen our understanding of plant–*Trichoderma* interactions. Transcriptome analysis of the *T. virens*–maize interaction revealed the upregulation of coexpressed genes of diverse *Trichoderma* gene clusters for biosynthesis of specialized metabolites (Lawry 2016) (Supplementary Fig. S1). For example, *tv2og1* (within cluster 1) encodes a putative protein with a 2-oxoglutarate (2OG)-Fe(II)-dependent dioxygenase domain. Gene *vir4* (within cluster 2, called the *vir4* cluster) encodes one of the diverse putative terpene synthases described for *Trichoderma* spp. (Vicente et al. 2020). The knockout of *tv2og1* diminishes the ability of *T. virens* to colonize maize roots and has an impact on fungal iron regulation (G. Nogueira-López, M. Rostás, J. M. Steyaert, J. Hampton, and A. Mendoza-Mendoza, unpublished), while the knockout of *vir4* inhibits the biosynthesis of many terpenes in *T. virens* (Crutcher et al. 2013). Thus, Δ*tv2og1* and Δ*vir4* knockout mutants are particularly useful to test how the corresponding genes may affect fungal and plant metabolism.

In this study, metabolomics and gene expression analyses were applied to investigate changes occurring in the maize–*T. virens* interaction at an early developmental stage, focusing on specialized metabolism. Three *T. virens* genotypes—namely, the wild type (WT) and two knockout mutants, Δ*tv2og1* and Δ*vir4*—were used to elucidate (i) the specificity of metabolic responses occurring in colonized roots and (ii) how the presence or absence of the genes (*tv2og1* or *vir4*) modifies the intracellular and extracellular (secreted) metabolome of *T. virens*. In addition to metabolic fingerprints, several amino acids, flavonoids, and benzoxazinoids were targeted. The latter are characteristic specialized metabolites of maize (Zhou et al. 2018). We show that *T. virens* profoundly modulates the maize root metabolome. These changes depend on the genotype of the fungus. Likewise, fungal metabolomes differed between the genotypes, indicating that both plant and fungal metabolites play essential roles during the symbiosis.

RESULTS

Colonization of maize roots by *T. virens*.

Surface-sterilized maize seeds were left untreated (control) or were inoculated with fungal conidia of different genotypes (WT, Δ*tv2og1*, or Δ*vir4*) of the *T. virens* strain Gv29.8. Seeds were germinated for 2.5 days, seedlings were grown in hydroponics for another 2.5 days, and roots were then harvested (i.e., 5 days post-inoculation [dpi]). Fungal root colonization (endophytic and rhizoplane colonization) was quantified by quantitative PCR (qPCR) using the genes encoding *actin* and *phenylalanine ammonia lyase* (*PAL*) as fungal and maize reference genes, respectively. The ratio of *actin*/*PAL* (*T. virens*/*Z. mays)* was determined in the primary root pieces. The genotypes Δ*tv2og1* and Δ*vir4* colonized the maize roots significantly less than the WT did (Fig. 1A).

The ability of the *T. virens* genotypes to endophytically colonize the maize roots was also tested by using surface-sterilized roots, which were sectioned and plated on *Trichoderma*-selective medium. All *T. virens* genotypes colonized the maize roots (Fig. 1B). A visual inspection of the plants revealed that maize growth was negatively affected by the presence of each of the three *T. virens* genotypes when compared with the untreated control plants (Fig. 1C).

The *T. virens*–maize root metabolome depends on the fungal genotype.

To study metabolites modulated by the *Trichoderma*–maize interaction, polar (90% methanol) extracts of roots of untreated plants or roots colonized with one of the *T. virens* genotypes (WT, Δ*tv2og1*, or Δ*vir4*) were subjected to untargeted metabolic fingerprinting. This was done using ultra-high performance liquid chromatography coupled to diode array detection and quadrupole time-of-flight tandem mass spectrometry in negative electrospray ionization mode (UHPLC-DAD-ESI$^-$-QTOF-MS/MS). Data are presented as metabolic "features", with each feature being characterized by its retention time and the mass-to-charge ratio (*m/z*) of the most intense ion found in the corresponding cluster of features belonging to the same metabolite. The raw data and feature tables will be made available shortly after publication of the study in the MetaboLights repository (Haug et al. 2013 [accession number MTBLS1964]). In total, 512 metabolic features were reliably found (i.e., present in many replicates and distinct from the blanks) in maize roots. These included 256 features present in the control plants and 377, 379, and 345 features in plants colonized with the *T. virens* genotypes WT, Δ*tv2og1*, and Δ*vir4*, respectively. In a principal component (PC) analysis (PCA), the first two axes explained about 34% of the total variance in the data (Fig. 2A). Along the first PC (PC 1), the metabolomes of control roots and *T. virens*-colonized roots were well separated, whereas the metabolomes of roots colonized by the different *T. virens* genotypes were separated along PC 2 (Fig. 2A).

To trace effects of *T. virens* colonization on individual metabolic features, two thresholds to define features as being modulated by the interaction compared with untreated plants were implemented. These were a significant difference between treatment and control ($P < 0.05$) according to Mann-Whitney *U* tests and a mean fold change of <0.5 or >2 for decreased and increased features, respectively. According to these thresholds,

67 and 273 features were decreased and increased in pool size, respectively, by the colonization of at least one of the *T. virens* genotypes. Colonization by the three genotypes of *T. virens* induced similar responsiveness (i.e., percentage of modulated compared with all features), regarding decreased metabolic features (Fig. 2B). However, about three to four times more features were increased than decreased by the colonization with *T. virens*. The highest number of increased features was found in plants colonized with the WT genotype (Fig. 2B). Several features were commonly decreased (30 features) but more than three times more features were commonly increased (94 features) due to colonization with all three *T. virens* genotypes. These commonly increased features represent a general response in the *T. virens*–maize interaction (Fig. 2C). In addition, specific responses to colonization by each *T. virens* genotype were detected (Fig. 2C). Taken together, metabolic fingerprinting revealed that the three *T. virens* genotypes profoundly modulated the metabolome of colonized maize roots in a genotype-specific manner.

The *T. virens* genotypes differ in their metabolomes.

After growing in a liquid medium, the dry mycelia biomass of the three fungal genotypes did not differ significantly ($n = 9$ replicates used for metabolic fingerprinting included; analysis of variance [ANOVA], $F_{2,24} = 1.32$, $P = 0.286$). To study whether fungal metabolomes are genotype-specific, metabolic fingerprinting of polar extracts of mycelia (intracellular fungal metabolome) and fungal culture supernatants (extracellular fungal metabolome) was performed as described above for roots. Across all three genotypes, 551 metabolic features were found in the mycelia, while 2,380 occurred in fungal culture supernatants. In the PCA of the mycelia data, the first two PCs explained about 39% of the variance in the data and the metabolomes of the three fungal genotypes were separated along PC 1 with a slight overlap between the mycelial metabolomes of WT and Δ*vir4* (Fig. 3A, left). For the fungal culture supernatants, the first two axes of the PCA explained about 53% of the variance and the three genotypes were separated with a slight overlap of a few samples (Fig. 3A, right).

To further trace metabolic differences between the fungal genotypes, concentrations of metabolic features in Δ*tv2og1* and Δ*vir4* were compared with those in the WT (Fig. 3B). Many features were more abundant in the Δ*tv2og1* compared with the WT mycelia samples, whereas fewer features differed between the Δ*vir4* and the WT genotype (Fig. 3B, left). In contrast, for the extracellular metabolome (fungal culture supernatants), both mutants showed various features with decreased concentrations compared with the WT (Fig. 3B, right). In the mycelial metabolomes, the three genotypes shared 201 metabolic features (36% of all detected features), while only 77 features (3%) were common in the fungal culture supernatants of the genotypes (Fig. 3C). Overall, metabolic fingerprinting of the three *T. virens* genotypes revealed pronounced differences in the metabolic composition of the mycelia and fungal culture supernatants. Indeed, large parts of both the intracellular and particularly the extracellular metabolome were genotype-specific.

Specific metabolic changes in the *T. virens*–maize interaction.

Several primary and specialized metabolites were putatively identified as aromatic amino acids (L-phenylalanine [L-PHE] and L-tryptophan [L-TRP]), benzoxazinoids (2-b-D-glucopyranosyloxy-4-hydroxy-1,4-benzoxazin-3-one [DIBOA glucoside], 2-b-D-glucopyranosyloxy-7-methoxy-1,4-benzoxazin-3-one [DIBOA-glucoside], 2-b-D-glucopyranosyloxy-7-methoxy-1,4-benzoxazin-3-one [HMBOA-glucoside], 2-b-D-glucopyranosyloxy-4-hydroxy-7-methoxy-1,4-benzoxazin-3-one [DIMBOA-glucoside], 2,4-dihydroxy-7-methoxy-1,4-benzoxazin-3-one [DIMBOA], 6-methoxy-benzoxazolin-2-one [MBOA], 2-b-D-glucopyranosyloxy-4,7-dimethoxy-1,4-benzoxazin-3-one [HDMBOA-glucoside], and 2-b-D-glucopyranosyloxy-4,7,8-trimethoxy-1,4-benzoxazin-3-one [HDM_2BOA-glucoside]), and flavonoids (naringenin, apigenin, tricin, and a dihydroxy-monomethoxy-flavone) (Table 1). The amino acids occurred in control and *T. virens*-colonized maize roots as well as in mycelia of all *T. virens* genotypes (Fig. 4). Whereas the concentration of L-TRP did not differ among treatment groups, the concentration of L-PHE was significantly higher in the control roots than in *T. virens*-colonized roots. No significant differences in the concentrations of L-TRP and

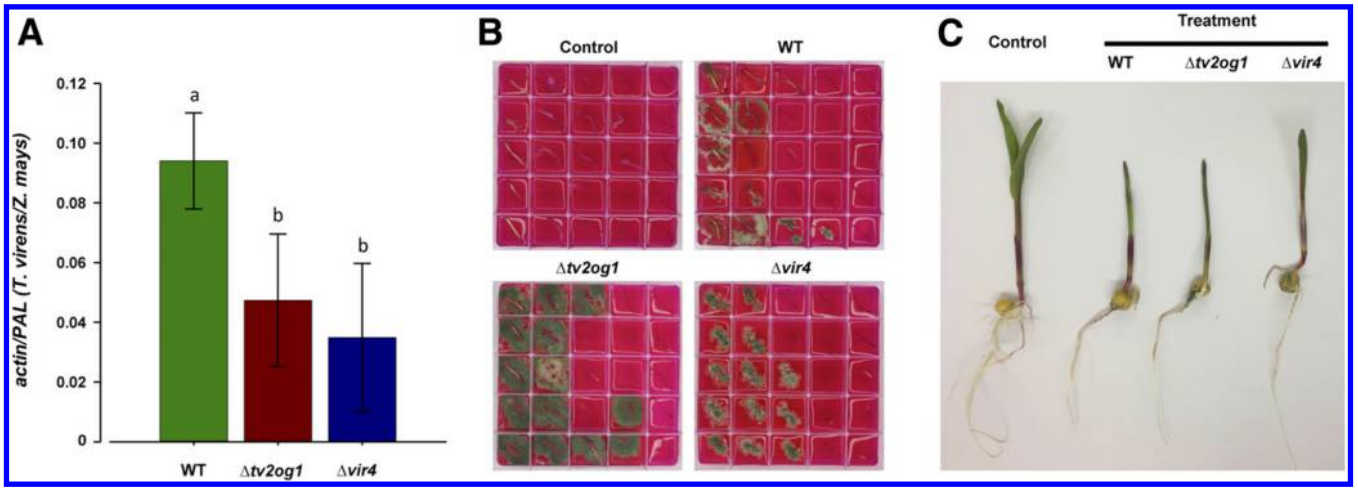

Fig. 1. Root colonization and appearance of maize seedlings grown in hydroponics after seed inoculation with different genotypes of *Trichoderma virens* (wild type [WT], Δ*tv2og1*, or Δ*vir4*). **A,** Colonization of roots by *T. virens*, measured as the ratio of fungal *actin* to maize *phenylalanine ammonia lyase* (*PAL*) in genomic DNA of primary root sections. Data represent means ± standard deviations of $n = 3$ biological replicates consisting each of four root samples from different plants. Different letters indicate significant differences between groups (analysis of variance with Bonferroni's post hoc test) at $P < 0.05$. **B,** Endophytic colonization by *T. virens*. Surface-sterilized primary root sections were placed on *Trichoderma*-selective medium for 7 days to observe fungal growth from these sections. Each row represents the five sections taken from one seedling. Root sections of the five replicates that are shown are representative for two independent experiments with $n = 9$ biological replicates each. **C,** Untreated (control) plants and plants colonized by *T. virens* genotypes 5 days postinoculation.

L-PHE in fungal mycelia were found among *T. virens* genotypes (Fig. 4A). The benzoxazinoids were detected in both the control and *T. virens*-colonized roots but not in mycelia or fungal culture supernatants. DIBOA-glucoside was less abundant in roots colonized by *T. virens*, with the Δ*vir4*-colonized roots having significantly lower concentrations than control roots. The concentration of MBOA was significantly lower in roots colonized by the Δ*vir4* genotype compared with roots colonized by Δ*tv2og1*. HDM_2BOA-glucoside had significantly higher concentrations in roots colonized with the fungal WT than in control roots. No significant differences in the concentrations of HMBOA-glucoside, DIMBOA-glucoside, DIMBOA, and HDMBOA-glucoside were found between colonized and control roots (Fig. 4B).

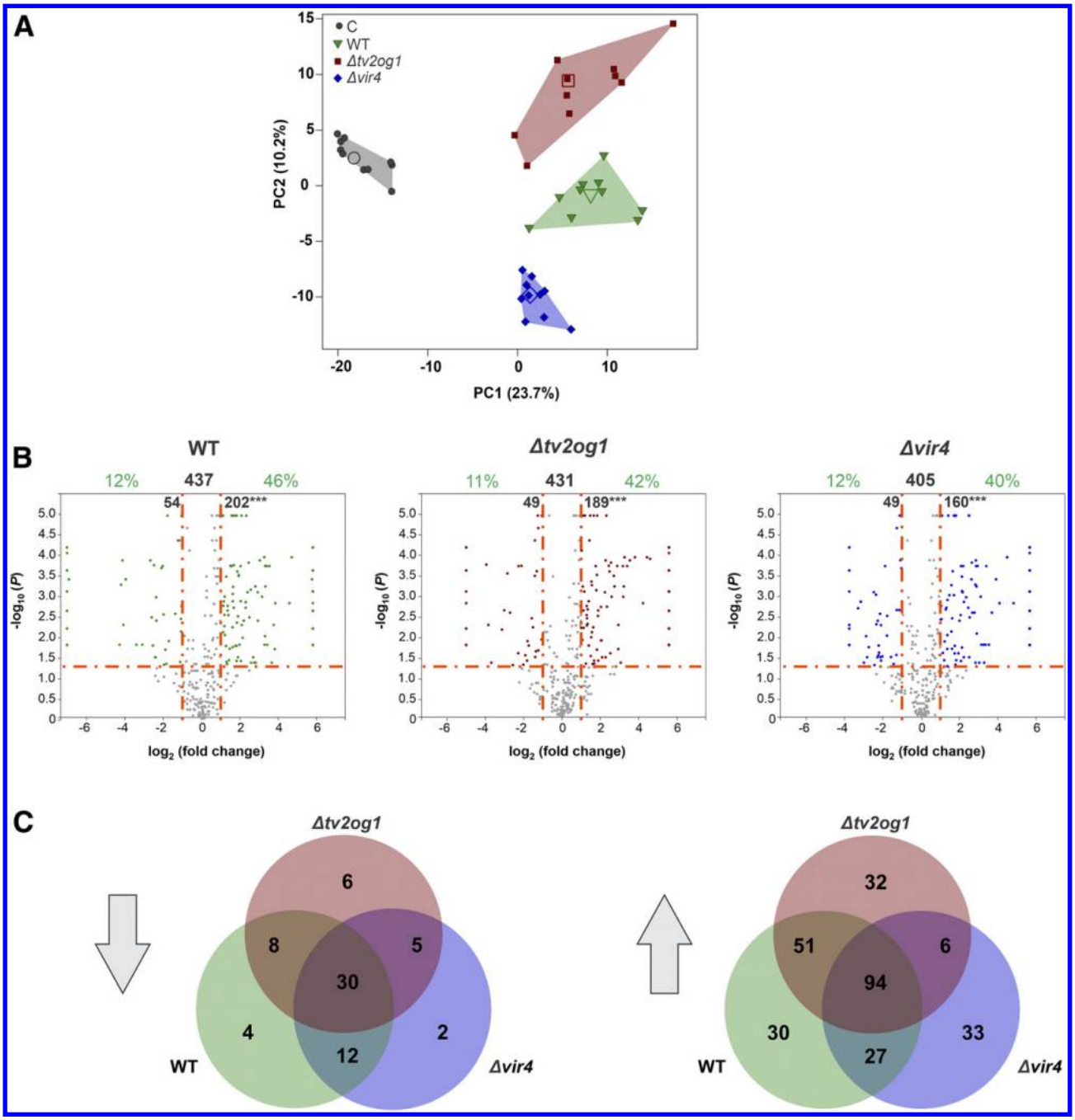

Fig. 2. Metabolic patterns of maize roots colonized with genotypes of *Trichoderma virens* (wild type [WT], Δ*tv2og1*, or Δ*vir4*) and untreated control roots (C) 5 days postinoculation. **A,** Score plot of a principal component (PC) analysis; 512 metabolic features were included, zeros replaced by random small numbers, and data autoscaled. Total variances explained by the first two PCs are given in parentheses; median scores are shown as larger, open symbols for each treatment; and groups are surrounded by convex hulls. **B,** Features modulated by colonization with *T. virens* genotypes shown as colored circles outside the cut-off lines (Mann Whitney *U* test: *P* value < 0.05; fold change < 0.5 for decreased features and > 2 for increased ones) in volcano plots. Features in the left parts of the plots had lower concentrations in *T. virens*-colonized roots compared with control plants, whereas those in the right parts had higher concentrations. For features that only occurred in one of the treatment groups, fold changes were set to the maximum values (for decrease or increase) found in the pairwise comparison. Bold numbers (top center) represent the total number of features found for each treatment comparison. Green numbers represent the metabolic responsiveness (percentage of modulated related to all detected features) for decreased and increased features. Asterisks indicate significant differences according to χ^2 tests comparing the numbers of decreased versus increased features for each treatment pair (***, $P < 0.001$). **C,** Features modulated (left: decreased and right: increased) due to colonization by all *T. virens* genotypes or specifically by one or two genotypes, presented as Venn diagrams; $n = 10$ biological replicates.

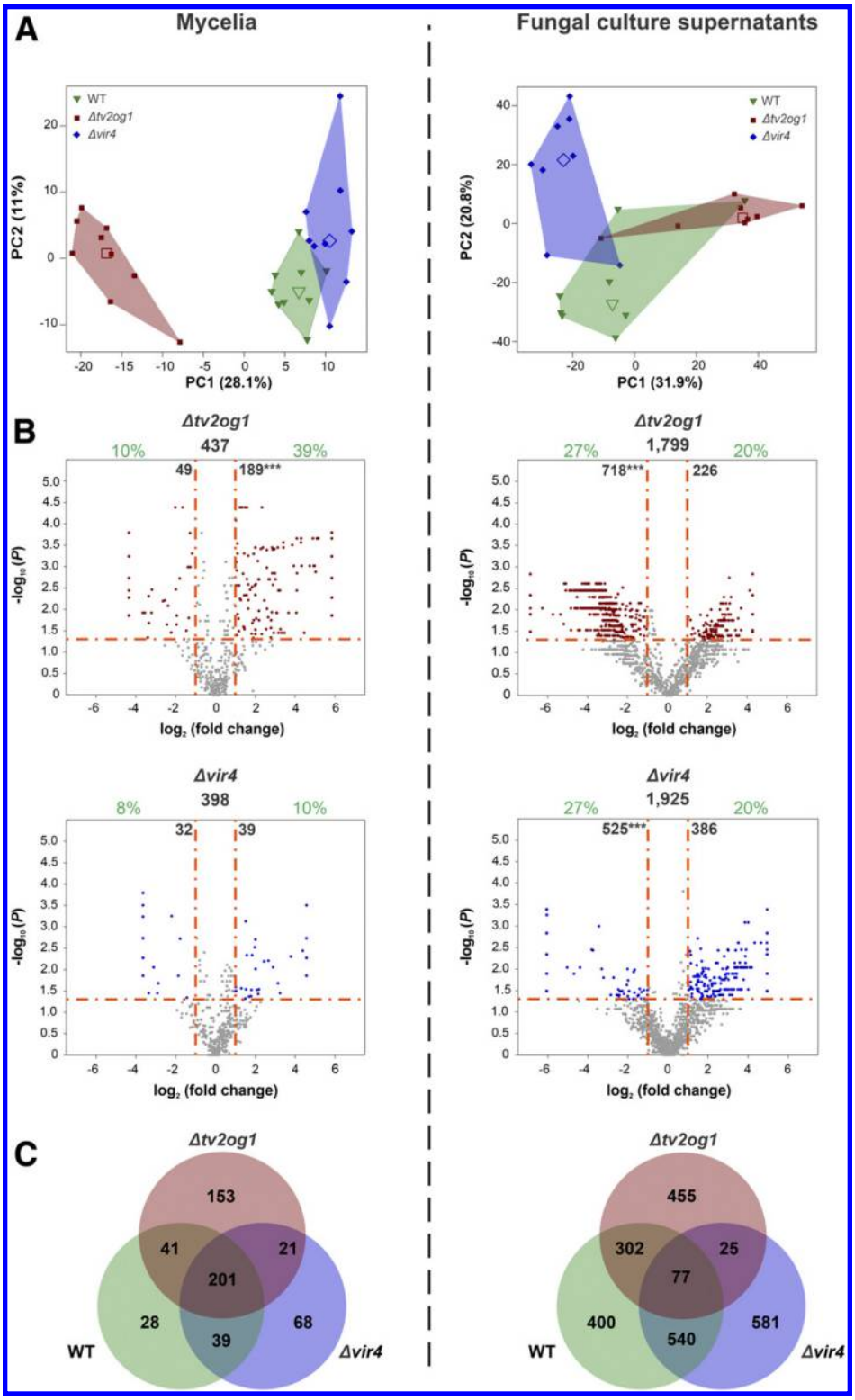

Fig. 3. Metabolic patterns of mycelia (left) and fungal culture supernatants (right) of *Trichoderma virens* (wild type [WT], Δ*tv2og1*, or Δ*vir4*). **A,** Score plots of principal component (PC) analyses; 551 and 2,380 metabolic features were included for mycelia and fungal culture supernatants, respectively; zeros were replaced by random small numbers and data autoscaled. Total variances explained by the first two PCs are given in parentheses; median scores are shown as larger, open symbols for each treatment; and groups are surrounded by convex hulls. **B,** Features modulated by deletion of *tv2og1* or *vir4* in comparison with the WT genotype (parental strain), shown as colored circles outside the cut-off lines (Mann Whitney *U* test: *P* value < 0.05; fold change < 0.5 for decreased features and > 2 for increased ones) in volcano plots. Features on the left sides of the plots had lower concentrations in the mutant than in the WT genotype, whereas those on the right sides had higher concentrations. For features that only occurred in one of the treatment groups, fold changes were set to the maximum values (for decrease or increase) found in the pairwise comparison. Bold numbers (top center) represent the total number of features found for each treatment comparison. Green numbers represent the metabolic responsiveness (percentage of modulated related to all detected features) for decreased and increased features. Asterisks indicate significances according to χ^2 tests comparing the numbers of decreased versus increased features for each genotype pair (***, $P <$ 0.001). **C,** Number of metabolic features occurring in the fungal genotypes presented as Venn diagrams; $n = 9$ and $n = 8$ biological replicates for mycelia and fungal culture supernatants, respectively.

Table 1. Metabolites identified in maize roots colonized by *Trichoderma virens*

Metabolite[a]	Molecular formula	Retention time (min)	*m/z*[b]	Ions[c]
Amino acids				
L-Phenylalanine	$C_9H_{11}NO_2$	2.00	**164.072**	**[M-H]$^-$**
	…	…	147.044	[$C_9H_7O_2$]$^-$
	…	…	103.055	[C_8H_7]$^-$
	…	…	91.055	[C_7H_7]$^-$
L-Tryptophan	$C_{11}H_{12}N_2O_2$	3.26	**203.083**	**[M-H]$^-$**
	…	…	142.065	[$C_{10}H_8N$]$^-$
	…	…	116.050	[C_8H_6N]$^-$
Benzoxazinoids				
DIBOA-glucoside	$C_{14}H_{17}NO_9$	6.10	**342.083**	**[M-H]$^-$**
	…	…	162.019	[$C_8H_4NO_3$]$^-$
	…	…	134.024	[$C_7H_4NO_2$]$^-$
HMBOA-glucoside	$C_{15}H_{19}NO_9$	7.39	**356.099**	**[M-H]$^-$**
	…	…	194.046	[$C_9H_8NO_4$]$^-$
	…	…	166.051	[$C_8H_8NO_3$]$^-$
	…	…	148.040	[$C_8H_6NO_2$]$^-$
	…	…	138.056	[$C_7H_8NO_2$]$^-$
	…	…	123.032	[$C_6H_5NO_2$]$^-$
DIMBOA-glucoside	$C_{15}H_{19}NO_{10}$	7.60	**745.195**	**[2M-H]$^-$**
	…	…	418.100	[M+HCOOH-H]$^-$
	…	…	372.094	[M-H]$^-$
	…	…	210.041	[$C_9H_8NO_5$]$^-$
	…	…	192.030	[$C_9H_6NO_4$]$^-$
	…	…	164.036	[$C_8H_6NO_3$]$^-$
	…	…	149.012	[$C_7H_3NO_3$]$^-$
DIMBOA	$C_9H_9NO_5$	7.66	210.041	[M-H]$^-$
	…	…	**164.036**	**[$C_8H_6NO_3$]$^-$**
	…	…	149.012	[$C_7H_3NO_3$]$^-$
	…	…	121.017	[$C_6H_3NO_2$]$^-$
MBOA	$C_8H_7NO_3$	9.78	**164.035**	**[M-H]$^-$**
	…	…	149.012	[$C_7H_3NO_3$]$^-$
	…	…	121.017	[$C_6H_3NO_2$]$^-$
HDMBOA-glucoside	$C_{16}H_{21}NO_{10}$	10.38	773.226	[2M-H]$^-$
	…	…	**432.115**	**[M+HCOOH-H]$^-$**
	…	…	386.109	[M-H]$^-$
	…	…	356.098	[$C_{15}H_{18}NO_9$]$^-$
	…	…	224.056	[$C_{10}H_{10}NO_5$]$^-$
	…	…	194.046	[$C_9H_8NO_4$]$^-$
	…	…	164.035	[$C_8H_6NO_3$]$^-$
	…	…	149.012	[$C_7H_3NO_3$]$^-$
HDM_2BOA-glucoside	$C_{17}H_{23}NO_{11}$	10.56	**462.126**	**[M+HCOOH-H]$^-$**
	…	…	254.066	[$C_{11}H_{12}NO_6$]$^-$
	…	…	224.056	[$C_{10}H_{10}NO_5$]$^-$
	…	…	194.045	[$C_9H_8NO_4$]$^-$
	…	…	179.023	[$C_8H_5NO_4$]$^-$
Flavonoids	…	…		
Naringenin	$C_{15}H_{12}O_5$	18.21	**271.061**	**[M-H]$^-$**
	…	…	177.019	[$C_9H_5O_4$]$^-$
	…	…	151.004	[$C_7H_3O_4$]$^-$
	…	…	119.050	[C_8H_7O]$^-$
	…	…	107.014	[$C_6H_3O_2$]$^-$
	…	…	93.034	[C_6H_5O]$^-$
Apigenin	$C_{15}H_{10}O_5$	19.19	**269.046**	**[M-H]$^-$**
	…	…	225.056	[$C_{14}H_9O_3$]$^-$
	…	…	151.004	[$C_7H_3O_4$]$^-$
	…	…	149.025	[$C_8H_5O_3$]$^-$
	…	…	117.035	[C_8H_5O]$^-$
Tricin	$C_{17}H_{14}O_7$	20.35	**329.067**	**[M-H]$^-$**
	…	…	314.045	[$C_{16}H_{10}O_7$]$^-$
	…	…	299.019	Unknown
Dihydroxy-monomethoxy-flavone	$C_{16}H_{12}O_5$	24.12	**283.061**	**[M-H]$^-$**
	…	…	268.038	[$C_{15}H_8O_5$]$^-$

[a] Metabolites that were validated via a reference standard are given in bold. DIBOA-glucoside = 2-b-D-glucopyranosyloxy-4-hydroxy-1,4-benzoxazin-3-one, HMBOA-glucoside = 2-b-D-glucopyranosyloxy-7-methoxy-1,4-benzoxazin-3-one, DIMBOA-glucoside = 2-b-D-glucopyranosyloxy-4-hydroxy-7-methoxy-1,4-benzoxazin-3-one, DIMBOA = 2,4-dihydroxy-7-methoxy-1,4-benzoxazin-3-one, MBOA = 6-methoxy-benzoxazolin-2-one, HDMBOA-glucoside = 2-b-D-glucopyranosyloxy-4,7-dimethoxy-1,4-benzoxazin-3-one, and HDM_2BOA-glucoside = 2-b-D-glucopyranosyloxy-4,7,8-trimethoxy-1,4-benzoxazin-3-one.

[b] Mass-to-charge ratios of ions that were visible in mass spectrometry (MS) mode and of fragments visible in MS mode (in-source fragmentation) or in tandem MS mode. Dominant *m/z* that were used for quantification and fragmentation are given in bold.

[c] Ion types that were visible in MS mode are shown. Ion formulas are given for fragments.

Changes in flux through metabolic pathways may result from changes in the expression of the genes encoding the enzymes involved in the corresponding metabolic steps or from changes in activities of enzymes. Therefore, key enzymes of the pathways (Figs. 4 and 5, shown in red) were analyzed for differences in gene expression between groups using reverse-transcription (RT)-qPCR. From the six genes which encode enzymes of the benzoxazinoid biosynthetic pathway, one (*BX10*) was upregulated in roots colonized by the *Δvir4* genotype of *T. virens* compared with control roots, whereas another gene (*Bx11*) showed a significantly higher expression in *Δvir4*-colonized roots compared with control and Δ*tv2og1*-colonized roots (Fig. 5A).

The three flavonoids naringenin, apigenin, and dihydroxy-monomethoxy-flavone were only found in roots colonized by *T. virens* but not in control roots, fungal mycelia, or fungal culture supernatants (Fig. 4C). The concentration of apigenin was significantly lower in roots colonized by the *Δvir4* genotype compared with roots colonized by the WT, whereas that of the dihydroxy-monomethoxy-flavone was significantly lower in roots colonized by the *Δvir4* genotype compared with roots colonized by Δ*tv2og1*. Tricin was detected in control and *T. virens*-colonized roots, with significantly higher concentrations in roots colonized with the fungal WT than in control roots. Compared with control roots, expression of the *PAL* gene from the flavonoid biosynthetic pathway was upregulated in roots colonized by the Δ*vir4* genotype but not in those colonized by the WT or Δ*tv2og1* genotypes (Fig. 5B). The flavone synthase I-encoding gene *ZmFNSI* showed significantly higher gene expression in roots colonized by the Δ*vir4* genotype than in those not colonized or colonized by the Δ*tv2og1* genotype. Gene expression of the second flavone synthase gene *ZmFNSII* did not significantly differ between groups (Fig. 5B). Thus, as for the overall metabolic fingerprints, responses in the fungus–plant interaction were highly fungal genotype-specific for both the annotated metabolites and the genes related to their biosynthesis.

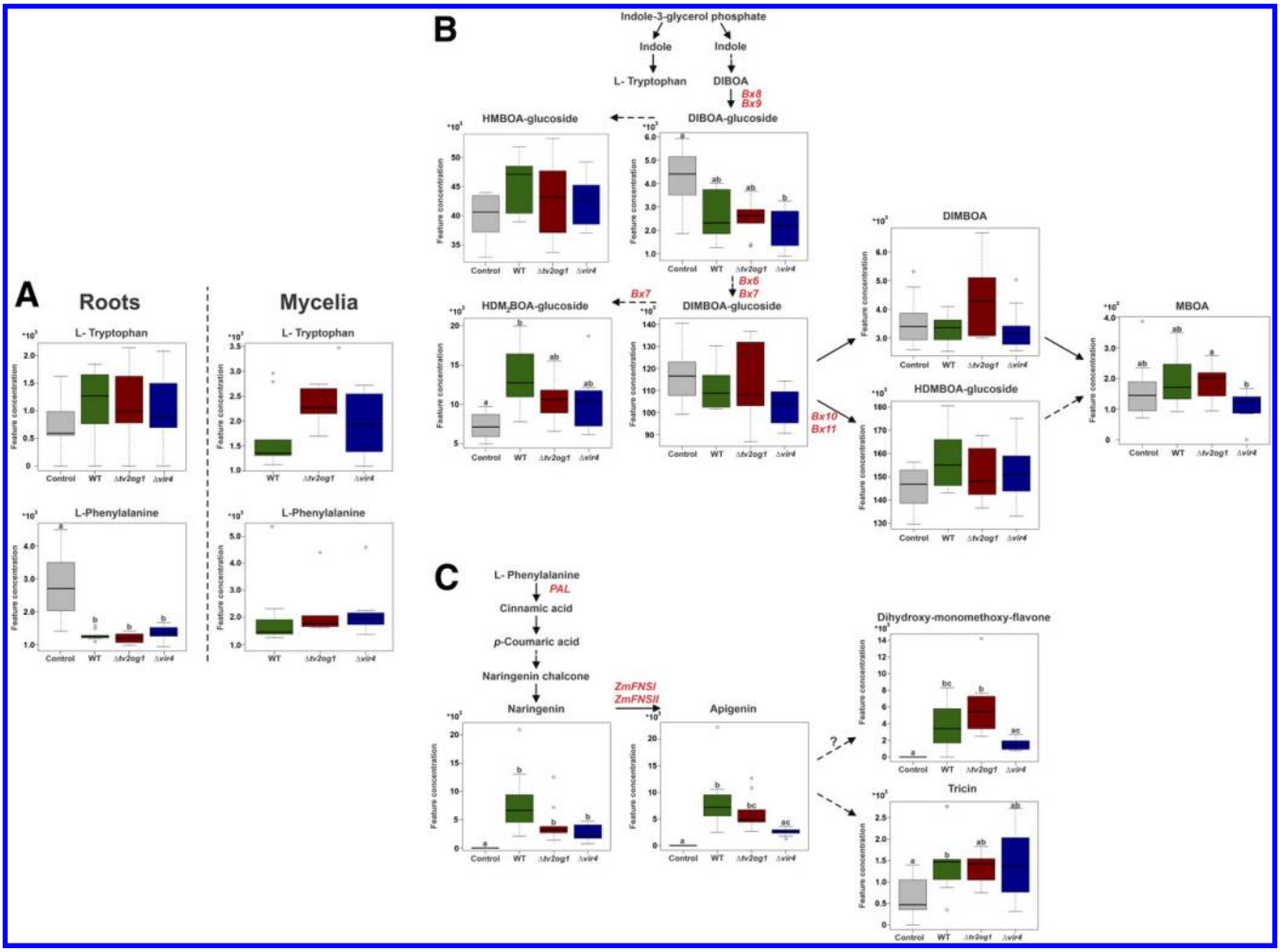

Fig. 4. Concentrations of metabolites (**A,** amino acids; **B,** benzoxazinoids; and **C,** flavonoids) identified in maize roots colonized with genotypes of *Trichoderma virens* (wild type [WT], *Δtv2og1*, or Δ*vir4*) and untreated control plants at 5 days postinoculation and in mycelia. Data are given as box-whisker plots showing the medians (horizontal lines), the interquartile ranges (IQR, boxes), outliers (open circles), and the whiskers (extending to a maximum 1.5× the IQR from the boxes). Different letters indicate significant differences between groups (Kruskal-Wallis tests followed by Kruskalmc tests) at $P < 0.05$. For **B** and **C**, Known biosynthetic connections for maize plants according to Cotton et al. (2019), Casas et al. (2014), and Lam et al. (2015) are shown; $n = 10$ biological replicates. HMBOA-glucoside = 2-b-D-glucopyranosyloxy-7-methoxy-1,4-benzoxazin-3-one, DIBOA-glucoside = 2-b-D-glucopyranosyloxy-4-hydroxy-1,4-benzoxazin-3-one, HDM_2BOA-glucoside = 2-b-D-glucopyranosyloxy-4,7,8-trimethoxy-1,4-benzoxazin-3-one, DIMBOA-glucoside = 2-b-D-glucopyranosyloxy-4-hydroxy-7-methoxy-1,4-benzoxazin-3-one, DIMBOA = 2,4-dihydroxy-7-methoxy-1,4-benzoxazin-3-one, HDMBOA-glucoside = 2-b-D-glucopyranosyloxy-4,7-dimethoxy-1,4-benzoxazin-3-one, and MBOA = 6-methoxy-benzoxazolin-2-one.

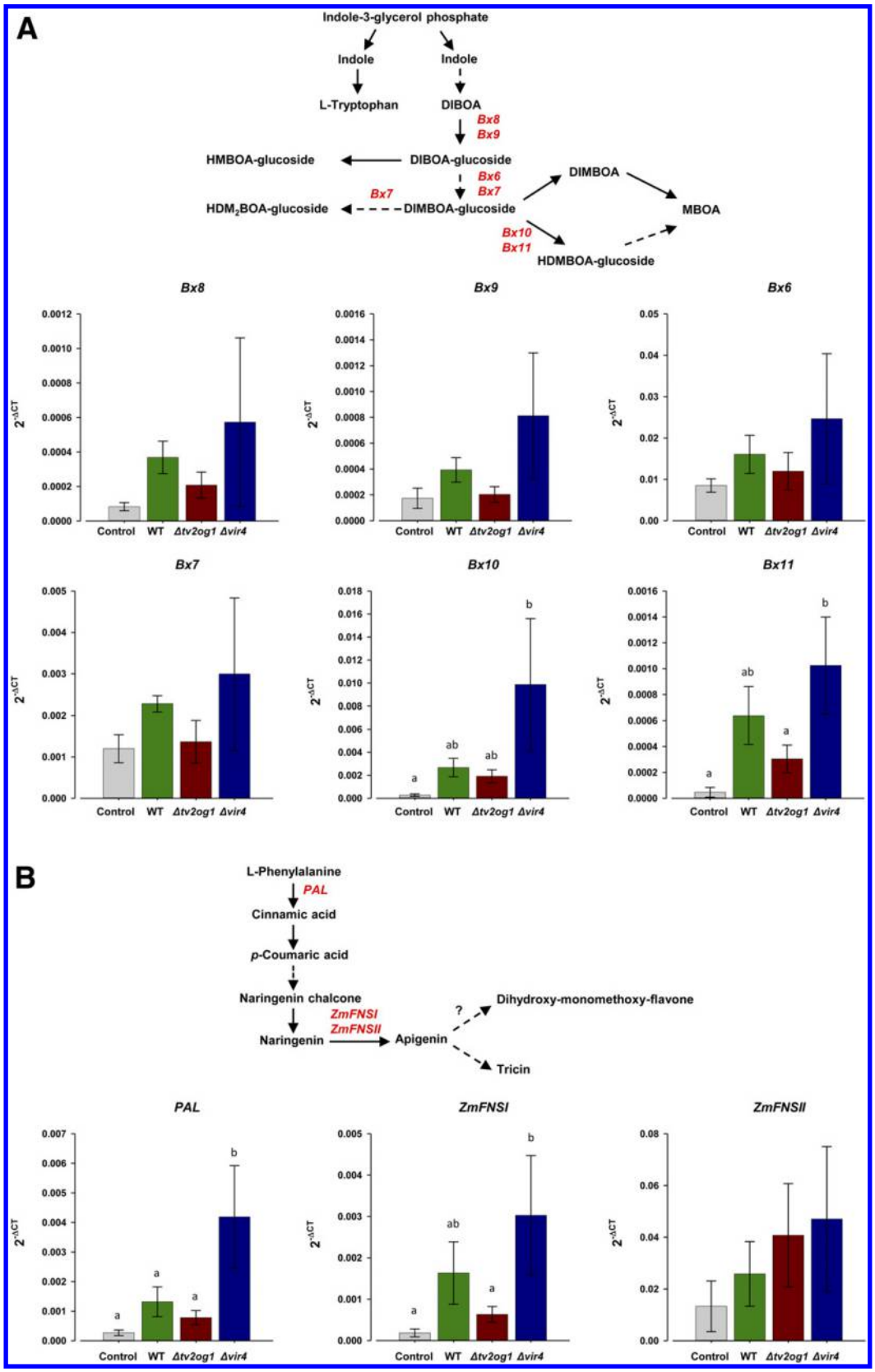

Fig. 5. Relative expression of genes encoding enzymes in metabolic pathways (**A,** benzoxazinoids and **B,** flavonoids) in maize roots colonized with genotypes of *Trichoderma virens* (wild type [WT], *Δtv2og1*, or Δ*vir4*) and untreated control plants 5 days postinoculation. Gene expression was measured by reverse-transcription quantitative PCR. Data are given as means ± standard deviations. Different letters indicate significant differences between groups (analysis of variance tests with Bonferroni's post hoc tests) at $P < 0.05$. Positions of the corresponding enzymes are indicated in red in the metabolic pathways in the upper panels; $n = 3$ biological replicates consisting of a pool of four roots from different plants each. HMBOA-glucoside = 2-b-D-glucopyranosyloxy-7-methoxy-1,4-benzoxazin-3-one, DIBOA-glucoside = 2-b-D-glucopyranosyloxy-4-hydroxy-1,4-benzoxazin-3-one, HDM_2BOA-glucoside = 2-b-D-glucopyranosyloxy-4,7,8-trimethoxy-1,4-benzoxazin-3-one, DIMBOA-glucoside = 2-b-D-glucopyranosyloxy-4-hydroxy-7-methoxy-1,4-benzoxazin-3-one, DIMBOA = 2,4-dihydroxy-7-methoxy-1,4-benzoxazin-3-one, HDMBOA-glucoside = 2-b-D-glucopyranosyloxy-4,7-dimethoxy-1,4-benzoxazin-3-one, MBOA = 6-methoxy-benzoxazolin-2-one, and *PAL* = *phenylalanine ammonia lyase.*

DISCUSSION

Colonization of maize roots by different *T. virens* genotypes and negative effects on maize plant growth.

In the current study, we observed that, in a hydroponic system, *T. virens* WT and the Δ*tv2og1* and Δ*vir4* knockout mutants colonized the maize roots but colonization levels by the fungal mutants were significantly lower (Fig. 1A). These lower levels indicate that *tv2og1* and *vir4* are important components for the root colonization in this system. Plants colonized by *T. virens* had less root and shoot biomass compared with the control plants at 5 dpi (Fig. 1C). Similarly, Nogueira-Lopez et al. (2018) and Rubio et al. (2012) showed that the same strain of *T. virens* that was used in the present study (Gv29.8) led to reduced growth of secondary roots and stems in maize and tomato seedlings, respectively. When interacting with *Arabidopsis thaliana*, diverse *Trichoderma* spp. suppress the growth of the primary root, although an enhanced biomass of secondary roots was observed (Nieto-Jacobo et al. 2017). These adverse effects on plant growth may be explained by competition for nutrients between the plant and the fungus under certain nutrient deficiencies (Li et al. 2015; Vinci et al. 2018) or the production of plant-growth-inhibiting molecules by *T. virens*. In addition, the induction of host cell death by the fungus as part of the colonization process may have played a role. Indeed, induction of cell death can help endophytes to proliferate, as shown for the fungus *Piriformospora indica* in the roots of barley (family Poaceae) (Deshmukh et al. 2006).

Pronounced metabolic differences between control and *T. virens*-colonized maize roots are fungal genotype-specific.

The metabolomes of maize roots colonized by *T. virens* differed distinctly from those of control roots, with many metabolic features being increased in concentration (Fig. 2). The large number of features that only occurred in or had higher concentrations in *T. virens*-colonized roots compared with control roots (Fig. 2B) could be due to the presence of fungal intra- and extracellular metabolites (Fig. 3), as it is well-known that *Trichoderma* spp. produce a plethora of specialized metabolites (Zeilinger et al. 2016). The observed changes in the metabolomes of colonized roots may also be due to the process of initiating and developing the plant–microbe interaction and may include the production and exchange of signaling compounds between the interaction partners. In the early stages of the induction of metabolic processes in maize roots, plant defense responses may be elicited by fungal compounds or by damage caused by plant cell wall digestion. With the development of the plant and the ongoing interaction, the effects and processes may change, as shown for other interactions between plants and beneficial microorganisms (Planchamp et al. 2015; Schweiger et al. 2014a; Zamioudis and Pieterse 2012).

In the specific case of *T. virens*–maize interactions, proteins released by the fungus were suggested to be responsible for successful colonization, such as potential effectors that may inhibit the synthesis of plant defense molecules (Nogueira-Lopez et al. 2018). Moreover, many changes in the metabolome are probably related to other effects of *Trichoderma* spp. on their host plants (Brotman et al. 2012; Vinci et al. 2018; Yedidia et al. 2003). For example, *Trichoderma* spp. are known to affect nutrient availabilities and uptake (Li et al. 2015), produce phytohormone-like substances (Guzmán-Guzmán et al. 2019), and increase photosynthesis (Harman et al. in press), which, in turn, could influence root metabolism.

Our study shows that *T. virens* modulated the metabolome of colonized maize roots in a genotype-dependent manner, with many features being altered by only one of the genotypes (Fig. 2). We found that the deletions of a gene encoding a putative protein with a 2OG-Fe(II)-dependent dioxygenase domain (*tv2og1*) or a terpene synthase (*vir4*) in *T. virens* profoundly affected the metabolome of *T. virens*-colonized roots. Because the fungal genotypes colonized the roots to different extents (Fig. 1A), part of the metabolic differences may be related to the proportions of mycelia in the roots. However, the huge qualitative and quantitative differences in the intra- and extracellular metabolites we observed for the different *T. virens* genotypes (Fig. 3) likely also made a large contribution. Because the mycelial growth in the liquid media was similar between the genotypes (data not shown), these differences seem to be directly related to fungal biosynthetic machineries rather than to differences in biomass production.

Proteins containing a 2OG-Fe(II)-dependent dioxygenase domain (e.g., *tv2og1*) are widespread in eukaryotes and prokaryotes. This superfamily of proteins is diverse and their members have multiple functions, including but not restricted to modifications of DNA and various specialized metabolites (Islam et al. 2018; Kawai et al. 2014). Several genes putatively encoding terpene synthases were described for *Trichoderma* spp., with indications that some of them play a role during colonization of host roots (Vicente et al. 2020). The gene *vir4* has been partially characterized, probably encoding a core enzyme for the biosynthesis of volatile terpenoids in *T. virens* (Crutcher et al. 2013). Interestingly, the current study shows that the deletion of the *vir4*-coding region also modifies the nonvolatile fungal metabolome. Overall, the high number of genotype-specific fungal metabolites suggests that the protein products of these two genes have far-reaching metabolic impacts and that pleiotropic effects may occur.

Annotated metabolites and their involvement in the *T. virens*–maize interaction.

The aromatic amino acids L-TRP and L-PHE found in both plant and fungal samples (Fig. 4A) are derived from the shikimate pathway. These amino acids are precursors of a broad range of specialized metabolites and hormones (Tzin and Galili 2010). In plants, the shikimate pathway is activated by several factors such as wounding, pathogens, and redox state (Tzin and Galili 2010). In the present study, these amino acids were found in roots and mycelium, indicating that the corresponding biosynthetic routes are expressed both in maize and *T. virens*.

The concentrations of L-TRP in maize roots were independent of colonization by *T. virens* (Fig. 4A). The benzoxazinoids, which are like L-TRP synthesized from indole (Cotton et al. 2019; Zhou et al. 2018), were only slightly affected by *T. virens* (Fig. 4B). In maize, benzoxazinoids are important defense-related metabolites (Ahmad et al. 2011; Niemeyer 2009). However, secreted benzoxazinoids can also act as attractants; for example, in the interaction of maize with the beneficial rhizobacterium *Pseudomonas putida* (Neal et al. 2012). The benzoxazinoid biosynthetic pathway is well described for plants (Cotton et al. 2019; Zhou et al. 2018) but there is no indication that fungi synthesize these metabolites. However, benzoxazinoid concentrations in maize plants can be modulated by diverse environmental factors, including fungi. For example, the AMF *Glomus mosseae* triggers the accumulation of DIMBOA in maize roots (Song et al. 2011) and levels of benzoxazinoids in maize roots and shoots are also influenced by different *Azospirillum* spp. and strains (Walker et al. 2011). Interestingly, DIMBOA UDP-glucosyltransferase (BX9), a key enzyme involved in the synthesis of benzoxazinoids, was found to be secreted into the apoplastic region of the primary roots of maize in the presence of *T. virens* after 5 days of interaction (Nogueira-Lopez et al. 2018). In the

present study, colonization of maize roots induced changes in the concentration of only a few benzoxazinoids, at least at the time point investigated. This low level of induction may be due to fungal compounds suppressing plant defense signaling. It would be interesting to investigate whether *T. virens* is capable of detoxifying benzoxazinoids, as described for *Fusarium verticillioides* (Glenn et al. 2003).

We found a lower concentration of L-PHE in *T. virens*-colonized roots than in control roots (Fig. 4A). This may indicate that the amino acid was incorporated into the specialized metabolism of the colonized roots to a greater extent than was the case in control roots, with its biosynthesis not being high enough to compensate for the increased demand. However, the expression of the gene coding for PAL, which mediates the conversion of L-PHE to cinnamic acid, was upregulated only in Δ*vir4*-colonized roots (Fig. 5B). Cinnamic acid is a precursor of diverse phenylpropanoids such as flavonoids and phenolic acids, which play essential roles in plant growth and development as well as in protection against stress (Deng and Lu 2017; Dixon and Paiva 1995). In *T. virens,* the gene cluster of the shikimate-chorismate catabolic pathway is upregulated during the interaction with maize roots (Lawry 2016). The fact that some flavonoids were found exclusively in *T. virens*-colonized roots indicates that L-PHE could have been used for their synthesis (Fig. 4C). These flavonoids may be involved in plant–fungus signaling or may be produced by the plant as a transient early defense response. Likewise, they could be involved in successful fungal colonization. Indeed, flavonoids display diverse biological activities in plants, including signaling, protection against abiotic stress, and facilitation of interactions with beneficial microbes (Cheynier et al. 2013; Harborne and Williams 2000; Mierziak et al. 2014). The flavonoid naringenin found in the *T. virens*-colonized roots may have been a critical factor for the establishment of the plant–fungus interaction. Naringenin has been associated with reduced lignin concentration in rice plants (Deng et al. 2004), which may facilitate the colonization of the internal root by the fungus. Furthermore, naringenin is known to inhibit the growth of different plant species, including maize (Deng et al. 2004). Therefore, it is conceivable that the growth inhibition of colonized roots observed in the present study (Fig. 1C) may be related to changes in naringenin.

Apigenin is derived from naringenin and known to occur in maize (Ferreyra et al. 2015). It shows antimicrobial activity against phytopathogenic fungi (Mierziak et al. 2014) and acts as a nematicide (Soriano et al. 2004). Thus, apigenin found in *T. virens*-colonized roots in the present study may modulate interactions of maize with various antagonists. The differences in the concentrations of apigenin between roots colonized by the *T. virens* genotypes WT and Δ*vir4* point toward a possible involvement of *vir4*-associated volatile terpenes in short-term regulation of the biosynthesis of certain flavonoids and in root colonization under nonaxenic conditions. Further studies are needed to test these hypotheses. Ferreyra et al. (2015) suggested that pathogens may induce flavone biosynthesis to reduce salicylic acid and, consequently, enhance susceptibility. The authors also proposed that apigenin could inhibit the enzymatic activities or the transcription of genes in the salicylic acid biosynthesis pathway. If this occurs during root colonization by *Trichoderma* spp., it would represent an interesting mechanism of plant immune suppression by nonpathogenic root colonizers that requires further investigation. Interestingly, naringin, a precursor of naringenin, was accumulated in leaves of bean plants inoculated with *T. velutinum* (Mayo-Prieto et al. 2019), suggesting that the biosynthesis of these flavonoids is induced in local and systemic tissues of plants treated with *Trichoderma* spp.

In monocots, tricin is an important monomer in the lignification process (Lan et al. 2015), which may be associated with the protection of roots against invaders, including beneficial microorganisms such as *Trichoderma* spp. Tricin can suppress soilborne pathogenic fungi such as *F. oxysporum* and *Rhizoctonia solani*, which cause rice seedling rot disease (Kong et al. 2010). If tricin does not affect *Trichoderma* growth, the induction of this flavonoid due to *Trichoderma* colonization may be an interesting mechanism of plant protection mediated by this endophyte. Indeed, flavonoids such as tricin induced by endophytic fungi have insecticidal activity (Ju et al. 1998; Mayo-Prieto et al. 2019), highlighting the multiple roles of these metabolites in interactions between organisms and their environment.

In general, the metabolite concentrations did not fit well to the expression of the genes that encode enzymes of the corresponding metabolic steps (Figs. 4 and 5). This may be due to time delays imposed by translation of transcripts or regulation of the activities of the enzymes via posttranslational modifications. Moreover, the accumulation of metabolites can induce a negative feedback on the transcription of the genes mediating the biosynthesis of these or other metabolites, leading to complex relationships between the metabolite and transcript levels across pathways. For example, increased concentrations of DIMBOA negatively affect the transcription of genes involved in the production of benzoxazinoids (Ahmad et al. 2011). The finding that some genes involved in specialized maize metabolism were upregulated by the *T. virens* genotype Δ*vir4* (Fig. 5) could indicate some involvement of the fungal *vir4* gene and its associated terpenes in the regulation of plant gene expression related to specialized metabolism during the interaction with the host.

By combining metabolomics and gene expression analyses of maize root–*T. virens* interactions, our study elucidated changes in overall metabolic patterns and uncovered the modulation of specific compounds characteristic for the symbiosis. Furthermore, our approach revealed pronounced differences in the metabolic patterns of colonized roots depending on the fungal genotype. The study supports previous findings that enzymes involved in fungal iron regulation and terpene synthesis play a role in the interaction with the host plant.

MATERIALS AND METHODS

Inoculum preparation.

Three genotypes of the *T. virens* strain Gv29.8—the WT; Δ*tv2og1* (G. Nogueira-López, M. Rostás, J. M. Steyaert, J. Hampton, and A. Mendoza-Mendoza unpublished); and Δ*vir4*, produced following the methodology described by Nogueira-López et al. (2019) for the deletion of *T. virens* terpene synthases—were propagated on potato dextrose agar (PDA) (Difco, Fisher Scientific, Newington, NH, U.S.A.) at 25°C under a cycle of 12 h of light and 12 h of darkness for 7 days to induce conidia formation (Supplementary Fig. S1). Conidia were collected in sterile Nanopure water and filtered through a double layer of sterile Miracloth (Millipore Merck, Boston, MA, U.S.A.).

Maize inoculation and germination.

Seeds of *Zea mays* of the hybrid line 34H31 (Pioneer Brand Products, Gisborne, New Zealand) were surface sterilized with 2% (wt/vol) sodium hypochlorite (NaOCl) and 70% ethanol as described by Nogueira-Lopez et al. (2018). Sterilized seeds were left untreated (as control) or inoculated with conidial suspensions (approximately 1×10^6 conidia/seed) of one of the genotypes of *T. virens* (WT, Δ*tv2og1*, or Δ*vir4*), and germinated for 2.5 days, as described by Nogueira-Lopez et al. (2018). The 2.5-day-old seedlings were transferred to hydroponic conditions

without aeration in 50-ml tubes containing 45 ml of sterile Hoagland's number 2 Basal Salt Mixture (Sigma-Aldrich, St. Louis, MO, U.S.A.) supplemented with 0.5% (wt/vol) sucrose with a piece of sterile cotton to support the seedling. Seedlings were set up in a randomized complete block design and incubated for an additional 2.5 days in a plant growth incubator (Humidity Control Versatile Environmental Test Chamber, Sanyo, Moriguchi, Japan) at 25°C under a cycle of 16 h of light and 8 h of darkness and relative humidity of 80%.

Determination of endophytic and rhizoplane colonization of maize roots by *T. virens*.

To quantify the root (endophytic and rhizoplane) colonization by *T. virens*, DNA was extracted from maize roots, and a *T. virens*-specific (*actin*) as well as a maize-specific (*PAL*) gene (Vargas et al. 2008) were quantified with qPCR. Primary roots were excised, gently washed with sterile Nanopure water, rinsed three times in sterile Nanopure water for 2 min, and ground into a fine powder in liquid nitrogen. Lysis buffer (500 µl of 2% Triton X, 1% sodium dodecyl sulfate, 100 mM NaCl, 10 mM Tris-HCl [pH 8.0], and 1 mM EDTA) and 500 µl of phenol-chloroform-isoamyl alcohol (25:24:1, vol/vol/vol) were added to 100 mg of root powder. Samples were vortexed for 10 s and centrifuged for 10 min (13,200 rpm, 4°C); then, supernatants were taken and mixed (five to six times inversion) with 2.5 volumes of 100% cold ethanol, and samples were centrifuged for 5 min (13,200 rpm, 4°C). Supernatants were discarded, samples were centrifuged for 2 min (13,200 rpm, 4°C), the remaining ethanol was removed, and the pellets were resuspended in 30 µl of ultrapure DNase/RNase-free distilled water. Samples were treated with 10 µl of RNase (Macherey-Nagel GmbH & Co. KG, Germany) for 15 min at 65°C. Isolated genomic DNA (gDNA) was quantified using a NanoDrop (Nanodrop Technologies, Montchanin, DE, U.S.A.).

The amplification mixture contained SsoAdvanced Universal SYBR Green Supermix (Bio-Rad Laboratories Inc., Hercules, CA, U.S.A.), 0.4 µM *T. virens*-specific (*actin*) and maize-specific (*PAL*) forward and reverse primers (Supplementary Table S1), and 200 ng of gDNA template in a 10-µl reaction volume. Amplification was carried out with an initial denaturation step at 95°C for 10 min, followed by 40 cycles at 95°C for 15 s, 60°C for 1 min, and capture during the extension phase of each cycle. Melt-curve analysis was carried out to confirm that a single product was amplified in each run. All reactions were run in triplicate and data of triplicate measurements were averaged later on.

Quantification of root colonization was performed based on a standard curve with five successive 10-fold dilution points of gDNA isolated from *T. virens* WT mycelium grown in liquid culture or maize roots using the DNA isolation protocol described above. Each dilution was analyzed by PCR using three technical replicates. The cycle threshold (CT) values for each DNA quantity were plotted to obtain the standard curve and the corresponding equation that was used for the quantification. The ratio of *actin* gDNA to *PAL* gDNA was calculated and compared between groups using an ANOVA with Bonferroni's post hoc test (Genstat, 19th Edition; VSN International, Hemel Hempstead, U.K.). Per *T. virens* genotype, $n = 3$ biological replicates, each consisting of four root samples collected from different plants, were used. The endophytic association of *T. virens* with maize plants (i.e., the internal colonization) was assessed as described by Mendoza-Mendoza et al. (2016), with modifications. Primary roots were excised, gently washed with sterile Nanopure water, soaked in 5% (wt/vol) NaOCl for 5 min for surface sterilization, and rinsed three times in sterile Nanopure water for 2 min. Primary roots were cut into five 1- to 2-cm pieces and placed in Petri dishes containing *Trichoderma*-selective medium (McLean et al. 2005). The Petri plates containing the root fragments were incubated at 25°C in the dark for 7 days to allow the endophyte to grow out of the roots. Roots of untreated maize seedlings were used as a control. Per *T. virens* genotype, $n = 9$ biological replicates were used and the experiment was set up twice.

Metabolic fingerprinting of roots, mycelia, and fungal culture supernatants.

For metabolic fingerprinting of maize roots, untreated plants (used as control) and plants inoculated with *T. virens* WT, Δ*tv2og1,* or Δvir4 were grown as described above ($n = 10$ biological replicates). The whole root system was excised, immediately frozen in liquid nitrogen, stored at –80°C, freeze-dried (Thermo Savant Micro Modulyo-115; Thermo Fisher Scientific, Waltham, MA, U.S.A.), and ground to a fine powder (1600 Mini6; SPEX SamplePrep, Metuchen, NJ, U.S.A.).

For chemical analyses of intra- and extracellular fungal metabolites, samples of mycelium and fungal culture supernatants were collected from cultures of the different fungal genotypes ($n = 10$ biological replicates). Conidia of *T. virens* (WT, Δ*tv2og1*, or Δ*vir4*) were harvested from 7-day-old PDA plates in 5 ml of sterile Nanopure water, filtered through two layers of sterile Miracloth, and incubated in 100-ml sterile flasks with 50 ml of Hoagland's number 2 Basal Salt Mixture supplemented with 0.5% sucrose. Flasks were incubated using a randomized complete block design at 25°C with shaking at 150 rpm (Ratek, Victoria, Australia). After 72 h, cultures were filtered through two layers of sterile Miracloth to separate the mycelia from the supernatants. Mycelia samples were frozen in liquid nitrogen and stored at –80°C. Supernatants were filtered through 0.2-µm membranes (GVS Filter Technology, Morecambe, U.K.) and stored at –80°C. Mycelia and supernatant samples were freeze-dried. Fungal tissue was ground to a fine powder. Samples of uninoculated sterile culture media ($n = 10$) were additionally stored for background subtraction (see below). Statistical analysis of fungal dry biomass was performed using ANOVA in R 3.4.1 (R Core Team).

For metabolic fingerprinting, 4 and 6 mg (± 0.1 mg) of (colonized) root and mycelial powder, respectively, were used. For the analysis of fungal culture supernatants, the freeze-dried material generated from the 50-ml cultures was used. Samples were extracted threefold on ice using 3 × 150 µl (roots), 3 × 50 µl (mycelia), or 3 × 200 µl (supernatants) of 90% ice-cooled methanol (LC-MS grade; Fisher Scientific, Loughborough, U.K.) containing hydrocortisone (>98%; Sigma-Aldrich, Steinheim, Germany) as internal standard. Samples were vortexed for 5 min and centrifuged for 10 min (13,200 rpm, 4°C). Supernatants were pooled and filtered using 0.2-µm filters (Phenomenex, Torrance, CA, U.S.A.). For each type of sample (roots, mycelia, and fungal culture supernatants), three to four blanks were prepared.

Samples and blanks were analyzed using UHPLC-DAD-QTOF-MS/MS (UHPLC: Dionex UltiMate 3000; Thermo Fisher Scientific, San José, CA, U.S.A.; and QTOF: compact; Bruker Daltonics, Bremen, Germany). Compounds were separated at 45°C on a Kinetex XB-C18 column (1.7 µm, 150 × 2.1 mm, with a precolumn; Phenomenex). Separation was performed using a gradient from eluent A (0.1% formic acid [FA; eluent additive for LC-MS, approximately 98%; Sigma-Aldrich] in Millipore-H_2O) to eluent B (0.1% FA in acetonitrile [LC-MS grade; Fisher Scientific]) at a flow rate of 0.5 ml min^{-1} with 2% B to 30% B within 20 min, 30% B to 75% B within 9 min, followed by column washing and equilibration. DAD spectra (210 to 400 nm) as well as mass line spectra (ESI^- mode, 8 Hz spectra rate, 50 to 1,500 *m/z* in both MS and MS/MS mode) were recorded. The MS parameters were end

plate offset 500 V, capillary voltage 3,000 V, nebulizer (N_2) pressure 3 bar, N_2 dry gas flow 12 liter min^{-1} at 275°C, quadrupole ion energy 4 eV, low mass 90 *m/z*, and collision energy 7 eV. MS/MS spectra were acquired in AutoMS/MS mode using N_2 as collision gas and 25 eV collision energy. A sodium formate-based calibration solution was pumped into the sprayer prior to each sample for mass axis recalibration. In total, $n = 9$ mycelia and $n = 8$ fungal culture supernatant samples were measured.

Mass axis recalibration was done individually for each sample. Picking of molecular features and spectral background subtraction were performed using the Find Molecular Features algorithm in Compass DataAnalysis 4.4 (Bruker Daltonics) with the following settings: signal-to-noise ratio 3, correlation coefficient threshold 0.75, minimum compound length 25 (roots) or 30 (mycelia and supernatant), smoothing width 7, allowing common adducts and neutral losses for bucket generation. Features were aligned across all samples (including root, mycelia, and fungal culture supernatant samples) with Compass ProfileAnalysis 2.3 (Bruker Daltonics), allowing deviations of 0.1 min (retention time) and 5 mDa (*m/z*), and using the *m/z* with the highest intensity as the bucketing basis. The peak heights of the features (each characterized by a retention time and *m/z* value) were normalized to the peak heights of the FA adduct of hydrocortisone. Two filtering steps were applied separately for each data set (i.e., colonized roots, mycelia, and fungal culture supernatants). A feature was maintained in the corresponding data set, if (i) its mean intensity in at least one treatment group was more than 50 times higher than its mean intensity in the blanks and (ii) it occurred in at least half of the replicates of at least one treatment group. For supernatant samples, those features that were present in the noninoculated culture media were not further considered (151 features). Data were normalized to the dry weights of the samples (except for the supernatant samples). For each data set, a PCA was performed using R 3.4.1 (R Core Team). For the PCAs, zeros were replaced by random small numbers (10^{-13} to 10^{-12}) and data autoscaled (i.e., mean centering and scaling to unit variance). For further pairwise group comparisons, only those features which occurred in at least half of the samples of at least one of the two treatment groups were retained. Volcano plots were plotted in Matlab (7.10.0.499; The MathWorks, Natick, MA, U.S.A.) based on fold changes of features (i.e., mean concentrations in the treatment group divided by mean concentrations in the control group) and *P* values resulting from Mann-Whitney *U* tests. For features that only occurred in one of the treatment groups, fold changes were set to the maximum fold change (for decrease or increase) observed in the corresponding data set. To compare the numbers of features decreased versus increased in pool size, χ^2 tests were performed in R. Venn diagrams were generated in R using the *gplots* package.

For identification of metabolites in the colonized roots, the annotation tools of Data Analysis 4.4 and MetaboScape 2.0 (Bruker Daltonics) were used. Molecular formulas of parent ions and fragments were generated using Smart Formula 3D and ranked according to their *m/z* and isotope pattern fit. For the most likely formulas, suggestions for structural formulas were derived from Compound Crawler and in silico fragmentation and matching against the MassBank of North America in MetFrag (Ruttkies et al. 2016). Moreover, dominant ion types, *m/z*, isotopic patterns, retention times, UV/VIS spectra, and MS/MS spectra were matched against an in-house database containing diverse primary and specialized metabolites that were measured under the same conditions. Ion types and *m/z* values of benzoxazinoids were additionally compared with those given by Bonnington et al. (2003) and Glauser et al. (2011). Features were screened for MS/MS similarities to known compounds to support metabolite identifications. For this, MetFamily (Treutler et al. 2016) as well as the bucket correlation statistics and the MS/MS bucket match function of MetaboScape were used. The concentrations of the identified metabolites were compared between treatment groups within each data set by Kruskal-Wallis tests followed by post hoc Kruskalmc tests in R (package *pgirmess*). Metabolic pathways for identified metabolites were obtained from Cotton et al. (2019), Casas et al. (2014), and Lam et al. (2015).

Gene expression measurements.

For total RNA extraction, roots were soaked and gently washed with sterile Nanopure water, and 2-cm sections nearest to the seed were cut from the primary roots and immediately frozen in liquid nitrogen. Total RNA was extracted using the TRIzol reagent (Invitrogen, Carlsbad, CA, U.S.A.) according to the manufacturer's instructions. RNA integrity was verified on denaturing 1% agarose gel prepared with 3-(morpholino) propane sulfonic acid buffer. The experiment was performed using $n = 3$ biological replicates per treatment, each containing a pool of four roots collected from different plants. Total RNA (2.5 µg per sample) was treated with ezDNase (Invitrogen) and reversely transcribed using SuperScript IV VILO master mix (Invitrogen) following the manufacturer's recommendations.

The expression levels of six genes of the benzoxazinoid biosynthetic pathway and three genes of the flavonoid pathway were quantified by RT-qPCR, using previously described gene-specific primers (Chen et al. 2016; Righini et al. 2019; Vargas et al. 2008; Von Rad et al. 2001; Wang et al. 2018) or primers that were designed using Primer3Plus software (Supplementary Table S1). All RT-qPCR assays were carried out in optical-grade 96-well plates (Axygen, Union City, CA, U.S.A.) on a StepOnePlus Real-Time PCR System (Applied Biosystems, Foster City, CA, U.S.A.). The amplification mixture contained SsoAdvanced Universal SYBR Green Supermix (Bio-Rad Laboratories Inc.), 0.4 µM forward and reverse primers (Supplementary Table S1), and 20 ng of cDNA template in 10 µl of reaction volume. Amplification was carried out with an initial denaturation step at 95°C for 10 min, followed by 40 cycles at 95°C for 15 s, 60°C for 1 min, and capture during the extension phase of each cycle. Melt-curve analysis was carried out to confirm that a single product was amplified in each run. All reactions were run in triplicate.

Relative gene expressions were calculated by relating the CT values of the target genes to those of the reference gene *β-tubulin* using the $2^{-\Delta CT}$ method (Schmittgen and Livak 2008), after CT values of triplicates were averaged for each biological replicate. For each gene, the relative gene expression was compared among groups using an ANOVA with Bonferroni's post hoc test with $P < 0.05$ (Genstat, 19th Edition).

ACKNOWLEDGMENTS

We thank A. Herrera-Estrella (Langebio, Mexico) for providing the *Trichoderma virens* strain Gv29.8; G. Glauser (University of Neuchâtel, Switzerland) and D. Sicker (University of Leipzig, Germany) for providing benzoxazinoid standards; the de.NBI MASH team (FKZ 031L0107), especially S. Neumann, K. Gorzolka, and R. Meier (Leibniz Institute of Plant Biochemistry, Halle, Germany), for bioinformatics support; and S. Neumann and the MetaboLights curation team for support with the publication of the data in MetaboLights.

AUTHOR-RECOMMENDED INTERNET RESOURCES

R Core Team 2017: https://www.r-project.org/
MassBank of North America: https://mona.fiehnlab.ucdavis.edu/
Primer3Plus software: https://primer3plus.com/

LITERATURE CITED

Agtuca, B. J., Stopka, S. A., Tuleski, T. R., do Amaral, F. P., Evans, S., Liu, Y., Xu, D., Monteiro, R. A., Koppenaal, D. W., Paša-Tolić, L., Anderton, C. R., Vertes, A., and Stacey, G. 2020. In-situ metabolomic analysis of *Setaria viridis* roots colonized by beneficial endophytic bacteria. Mol. Plant-Microbe Interact. 33:272-283.

Ahmad, S., Veyrat, N., Gordon-Weeks, R., Zhang, Y., Martin, J., Smart, L., Glauser, G., Erb, M., Flors, V., Frey, M., and Ton, J. 2011. Benzoxazinoid metabolites regulate innate immunity against aphids and fungi in maize. Plant Physiol. 157:317-327.

Andrade, S. A. L., Malik, S., Sawaya, A. C. H. F., Bottcher, A., and Mazzafera, P. 2013. Association with arbuscular mycorrhizal fungi influences alkaloid synthesis and accumulation in *Catharanthus roseus* and *Nicotiana tabacum* plants. Acta Physiol. Plant. 35:867-880.

Bonnington, L. S., Barcelò, D., and Knepper, T. P. 2003. Utilisation of electrospray time-of-flight mass spectrometry for solving complex fragmentation patterns: Application to benzoxazinone derivatives. J. Mass Spectrom. 38:1054-1066.

Brotman, Y., Landau, U., Cuadros-Inostroza, Á., Tohge, T., Fernie, A. R., Chet, I., Viterbo, A., and Willmitzer, L. 2013. *Trichoderma*-plant root colonization: Escaping early plant defense responses and activation of the antioxidant machinery for saline stress tolerance. PLoS Pathog. 9: e1003221.

Brotman, Y., Lisec, J., Méret, M., Chet, I., Willmitzer, L., and Viterbo, A. 2012. Transcript and metabolite analysis of the *Trichoderma*-induced systemic resistance response to *Pseudomonas syringae* in *Arabidopsis thaliana*. Microbiol. Read. 158:139-146.

Casas, M. I., Duarte, S., Doseff, A. I., and Grotewold, E. 2014. Flavone-rich maize: An opportunity to improve the nutritional value of an important commodity crop. Front. Plant Sci. 5:440.

Chen, L., Liu, Y., Wu, G., Veronican Njeri, K., Shen, Q., Zhang, N., and Zhang, R. 2016. Induced maize salt tolerance by rhizosphere inoculation of *Bacillus amyloliquefaciens* SQR9. Physiol. Plant. 158:34-44. 10.1111/ppl.12441

Cheynier, V., Comte, G., Davies, K. M., Lattanzio, V., and Martens, S. 2013. Plant phenolics: Recent advances on their biosynthesis, genetics, and ecophysiology. Plant Physiol. Biochem. 72:1-20.

Coppola, M., Diretto, G., Digilio, M. C., Woo, S. L., Giuliano, G., Molisso, D., Pennacchio, F., Lorito, M., and Rao, R. 2019. Transcriptome and metabolome reprogramming in tomato plants by *Trichoderma harzianum* strain T22 primes and enhances defense responses against aphids. Front. Physiol. 10:745.

Cotton, T. E. A., Pétriacq, P., Cameron, D. D., Meselmani, M. A., Schwarzenbacher, R., Rolfe, S. A., and Ton, J. 2019. Metabolic regulation of the maize rhizobiome by benzoxazinoids. ISME J. 13:1647-1658.

Crutcher, F. K., Parich, A., Schuhmacher, R., Mukherjee, P. K., Zeilinger, S., and Kenerley, C. M. 2013. A putative terpene cyclase, *vir4*, is responsible for the biosynthesis of volatile terpene compounds in the biocontrol fungus *Trichoderma virens*. Fungal Genet. Biol. 56:67-77.

Cruz-Magalhães, V., Nieto-Jacobo, M. F., van Zijll de Jong, E., Rostás, M., Padilla-Arizmendi, F., Kandula, D., Kandula, J., Hampton, J., Herrera-Estrella, A., Steyaert, J. M., Stewart, A., Loguercio, L. L., and Mendoza-Mendoza, A. 2019. The NADPH oxidases Nox1 and Nox2 differentially regulate volatile organic compounds, fungistatic activity, plant growth promotion and nutrient assimilation in *Trichoderma atroviride*. Front. Microbiol. 9:3271.

Deng, F., Aoki, M., and Yogo, Y. 2004. Effect of naringenin on the growth and lignin biosynthesis of gramineous plants. Weed Biol. Manage. 4: 49-55.

Deng, Y., and Lu, S. 2017. Biosynthesis and regulation of phenylpropanoids in plants. Crit. Rev. Plant Sci. 36:257-290.

De Palma, M., Salzano, M., Villano, C., Aversano, R., Lorito, M., Ruocco, M., Docimo, T., Piccinelli, A. L., D'Agostino, N., and Tucci, M. 2019. Transcriptome reprogramming, epigenetic modifications and alternative splicing orchestrate the tomato root response to the beneficial fungus *Trichoderma harzianum*. Hortic. Res. 6:5.

Deshmukh, S., Hückelhoven, R., Schäfer, P., Imani, J., Sharma, M., Weiss, M., Waller, F., and Kogel, K.-H. 2006. The root endophytic fungus *Piriformospora indica* requires host cell death for proliferation during mutualistic symbiosis with barley. Proc. Natl. Acad. Sci. U.S.A. 103: 18450-18457.

Dixon, R. A., and Paiva, N. L. 1995. Stress-induced phenylpropanoid metabolism. Plant Cell 7:1085-1097.

Druzhinina, I. S., Seidl-Seiboth, V., Herrera-Estrella, A., Horwitz, B. A., Kenerley, C. M., Monte, E., Mukherjee, P. K., Zeilinger, S., Grigoriev, I. V., and Kubicek, C. P. 2011. *Trichoderma*: The genomics of opportunistic success. Nat. Rev. Microbiol. 9:749-759.

Ferreyra, M. L. F., Emiliani, J., Rodriguez, E. J., Campos-Bermudez, V. A., Grotewold, E., and Casati, P. 2015. The identification of maize and Arabidopsis type I FLAVONE SYNTHASEs links flavones with hormones and biotic interactions. Plant Physiol. 169:1090-1107.

Fiehn, O., Kopka, J., Dörmann, P., Altmann, T., Trethewey, R. N., and Willmitzer, L. 2000. Metabolite profiling for plant functional genomics. Nat. Biotechnol. 18:1157-1161.

Glauser, G., Marti, G., Villard, N., Doyen, G. A., Wolfender, J.-L., Turlings, T. C. J., and Erb, M. 2011. Induction and detoxification of maize 1,4-benzoxazin-3-ones by insect herbivores. Plant J. 68:901-911.

Glenn, A. E., Meredith, F. I., Morrison, W. H., 3rd, and Bacon, C. W. 2003. Identification of intermediate and branch metabolites resulting from biotransformation of 2-benzoxazolinone by *Fusarium verticillioides*. Appl. Environ. Microbiol. 69:3165-3169.

Guzmán-Guzmán, P., Porras-Troncoso, M. D., Olmedo-Monfil, V., and Herrera-Estrella, A. 2019. *Trichoderma* species: Versatile plant symbionts. Phytopathology 109:6-16.

Harborne, J. B., and Williams, C. A. 2000. Advances in flavonoid research since 1992. Phytochemistry 55:481-504.

Harman, G. E., Doni, F., Khadka, R. B., and Uphoff, N. Endophytic strains of *Trichoderma* increase plants' photosynthetic capability. J. Appl. Microbiol. In press. doi.org/10.1111/jam.14368

Haug, K., Salek, R. M., Conesa, P., Hastings, J., de Matos, P., Rijnbeek, M., Mahendraker, T., Williams, M., Neumann, S., Rocca-Serra, P., Maguire, E., González-Beltrán, A., Sansone, S.-A., Griffin, J. L., and Steinbeck, C. 2013. MetaboLights—An open-access general-purpose repository for metabolomics studies and associated meta-data. Nucleic Acids Res. 41: D781-D786. 10.1093/nar/gks1004

Islam, M. S., Leissing, T. M., Chowdhury, R., Hopkinson, R. J., and Schofield, C. J. 2018. 2-Oxoglutarate-dependent oxygenases. Annu. Rev. Biochem. 87:585-620.

Ju, Y., Sacalis, J. N., and Still, C. C. 1998. Bioactive flavonoids from endophyte-infected blue grass (*Poa ampla*). J. Agric. Food Chem. 46: 3785-3788.

Kawai, Y., Ono, E., and Mizutani, M. 2014. Evolution and diversity of the 2-oxoglutarate-dependent dioxygenase superfamily in plants. Plant J. 78: 328-343.

Kong, C.-H., Xu, X.-H., Zhang, M., and Zhang, S.-Z. 2010. Allelochemical tricin in rice hull and its aurone isomer against rice seedling rot disease. Pest Manage. Sci. 66:1018-1024.

Lam, P. Y., Liu, H., and Lo, C. 2015. Completion of tricin biosynthesis pathway in rice: Cytochrome P450 75B4 is a unique chrysoeriol 5′-hydroxylase. Plant Physiol. 168:1527-1536.

Lamdan, N.-L., Shalaby, S., Ziv, T., Kenerley, C. M., and Horwitz, B. A. 2015. Secretome of *Trichoderma* interacting with maize roots: Role in induced systemic resistance. Mol. Cell. Proteomics 14: 1054-1063.

Lan, W., Lu, F., Regner, M., Zhu, Y., Rencoret, J., Ralph, S. A., Zakai, U. I., Morreel, K., Boerjan, W., and Ralph, J. 2015. Tricin, a flavonoid monomer in monocot lignification. Plant Physiol. 167:1284-1295.

Lawry, R. 2016. Cross-communication between Trichoderma and plants during root colonisation. Doctoral dissertation, Lincoln University, New Zealand.

Li, R.-X., Cai, F., Pang, G., Shen, Q.-R., Li, R., and Chen, W. 2015. Solubilisation of phosphate and micronutrients by *Trichoderma harzianum* and its relationship with the promotion of tomato plant growth. PLoS One 10:e0130081.

Marra, R., Ambrosino, P., Carbone, V., Vinale, F., Woo, S. L., Ruocco, M., Ciliento, R., Lanzuise, S., Ferraioli, S., Soriente, I., Gigante, S., Turrà, D., Fogliano, V., Scala, F., and Lorito, M. 2006. Study of the three-way interaction between *Trichoderma atroviride,* plant and fungal pathogens by using a proteomic approach. Curr. Genet. 50:307-321.

Martínez-Medina, A., Fernandez, I., Lok, G. B., Pozo, M. J., Pieterse, C. M. J., and Van Wees, S. C. M. 2017. Shifting from priming of salicylic acid- to jasmonic acid-regulated defences by *Trichoderma* protects tomato against the root knot nematode *Meloidogyne incognita*. New Phytol. 213:1363-1377.

Mayo-Prieto, S., Marra, R., Vinale, F., Rodríguez-González, Á., Woo, S. L., Lorito, M., Gutiérrez, S., and Casquero, P. A. 2019. Effect of *Trichoderma velutinum* and *Rhizoctonia solani* on the metabolome of bean plants (*Phaseolus vulgaris* L.). Int. J. Mol. Sci. 20:549.

McLean, K. L., Swaminathan, J., Frampton, C. M., Hunt, J. S., Ridgway, H. J., and Stewart, A. 2005. Effect of formulation on the rhizosphere competence and biocontrol ability of *Trichoderma atroviride* C52. Plant Pathol. 54:212-218.

Mendoza-Mendoza, A., Clouston, A., Li, J.-H., Nieto-Jacobo, M. F., Cummings, N., Steyaert, J., and Hill, R. 2016. Isolation and mass production of *Trichoderma*. Methods Mol. Biol. 1477:13-20.

Mhlongo, M. I., Piater, L. A., Madala, N. E., Labuschagne, N., and Dubery, I. A. 2018. The chemistry of plant-microbe interactions in the rhizosphere and the potential for metabolomics to reveal signaling related to defense priming and induced systemic resistance. Front. Plant Sci. 9:112.

Mierziak, J., Kostyn, K., and Kulma, A. 2014. Flavonoids as important molecules of plant interactions with the environment. Molecules 19: 16240-16265.

Morán-Diez, M. E., Trushina, N., Lamdan, N. L., Rosenfelder, L., Mukherjee, P. K., Kenerley, C. M., and Horwitz, B. A. 2015. Host-specific transcriptomic pattern of *Trichoderma virens* during interaction with maize or tomato roots. BMC Genomics 16:8.

Morath, S. U., Hung, R., and Bennett, J. W. 2012. Fungal volatile organic compounds: A review with emphasis on their biotechnological potential. Fungal Biol. Rev. 26:73-83.

Neal, A. L., Ahmad, S., Gordon-Weeks, R., and Ton, J. 2012. Benzoxazinoids in root exudates of maize attract *Pseudomonas putida* to the rhizosphere. PLoS One 7:e35498.

Niemeyer, H. M. 2009. Hydroxamic acids derived from 2-hydroxy-2*H*-1,4-benzoxazin-3(4*H*)-one: Key defense chemicals of cereals. J. Agric. Food Chem. 57:1677-1696.

Nieto-Jacobo, M. F., Steyaert, J. M., Salazar-Badillo, F. B., Nguyen, D. V., Rostás, M., Braithwaite, M., De Souza, J. T., Jimenez-Bremont, J. F., Ohkura, M., Stewart, A., and Mendoza-Mendoza, A. 2017. Environmental growth conditions of *Trichoderma* spp. affects indole acetic acid derivatives, volatile organic compounds, and plant growth promotion. Front. Plant Sci. 8:102.

Nogueira-López, G., Greenwood, D. R., Middleditch, M., Winefield, C., Eaton, C., Steyaert, J. M., and Mendoza-Mendoza, A. 2018. The apoplastic secretome of *Trichoderma virens* during interaction with maize roots shows an inhibition of plant defence and scavenging oxidative stress secreted proteins. Front. Plant Sci. 9:409.

Nogueira-López, G., Padilla-Arizmendi, F., Inwood, S., Lyne, S., Steyaert, J. M., Nieto-Jacobo, M. F., Stewart, A., and Mendoza-Mendoza, A. 2019. TrichoGate: An improved vector system for a large scale of functional analysis of *Trichoderma* genes. Front. Microbiol. 10:2794.

Peters, K., Worrich, A., Weinhold, A., Alka, O., Balcke, G., Birkemeyer, C., Bruelheide, H., Calf, O. W., Dietz, S., Dührkop, K., Gaquerel, E., Heinig, U., Kücklich, M., Macel, M., Müller, C., Poeschl, Y., Pohnert, G., Ristok, C., Rodríguez, V. M., Ruttkies, C., Schuman, M., Schweiger, R., Shahaf, N., Steinbeck, C., Tortosa, M., Treutler, H., Ueberschaar, N., Velasco, P., Weiß, B. M., Widdig, A., Neumann, S., and Dam, N. M. V. 2018. Current challenges in plant eco-metabolomics. Int. J. Mol. Sci. 19:1385.

Planchamp, C., Glauser, G., and Mauch-Mani, B. 2015. Root inoculation with *Pseudomonas putida* KT2440 induces transcriptional and metabolic changes and systemic resistance in maize plants. Front. Plant Sci. 5:719.

Righini, S., Rodriguez, E. J., Berosich, C., Grotewold, E., Casati, P., and Falcone Ferreyra, M. L. 2019. Apigenin produced by maize flavone synthase I and II protects plants against UV-B-induced damage. Plant Cell Environ. 42:495-508.

Rubio, M. B., Domínguez, S., Monte, E., and Hermosa, R. 2012. Comparative study of *Trichoderma* gene expression in interactions with tomato plants using high-density oligonucleotide microarrays. Microbiol. Read. 158:119-128.

Ruttkies, C., Schymanski, E. L., Wolf, S., Hollender, J., and Neumann, S. 2016. MetFrag relaunched: Incorporating strategies beyond *in silico* fragmentation. J. Cheminform. 8:3.

Schmittgen, T. D., and Livak, K. J. 2008. Analyzing real-time PCR data by the comparative C_T method. Nat. Protoc. 3:1101-1108.

Schweiger, R., Baier, M. C., and Müller, C. 2014a. Arbuscular mycorrhiza-induced shifts in foliar metabolism and photosynthesis mirror the developmental stage of the symbiosis and are only partly driven by improved phosphate uptake. Mol. Plant-Microbe Interact. 27:1403-1412.

Schweiger, R., Baier, M. C., Persicke, M., and Müller, C. 2014b. High specificity in plant leaf metabolic responses to arbuscular mycorrhiza. Nat. Commun. 5:3886.

Schweiger, R., and Müller, C. 2015. Leaf metabolome in arbuscular mycorrhizal symbiosis. Curr. Opin. Plant Biol. 26:120-126.

Shoresh, M., Harman, G. E., and Mastouri, F. 2010. Induced systemic resistance and plant responses to fungal biocontrol agents. Annu. Rev. Phytopathol. 48:21-43.

Simon, J. C., Marchesi, J. R., Mougel, C., and Selosse, M. A. 2019. Host-microbiota interactions: From holobiont theory to analysis. Microbiome 7:5.

Song, Y. Y., Cao, M., Xie, L. J., Liang, X. T., Zeng, R. S., Su, Y. J., Huang, J. H., Wang, R. L., and Luo, S. M. 2011. Induction of DIMBOA accumulation and systemic defense responses as a mechanism of enhanced resistance of mycorrhizal corn (*Zea mays* L.) to sheath blight. Mycorrhiza 21:721-731.

Soriano, I. R., Asenstorfer, R. E., Schmidt, O., and Riley, I. T. 2004. Inducible flavone in oats (*Avena sativa*) is a novel defense against plant-parasitic nematodes. Phytopathology 94:1207-1214.

Treutler, H., Tsugawa, H., Porzel, A., Gorzolka, K., Tissier, A., Neumann, S., and Balcke, G. U. 2016. Discovering regulated metabolite families in untargeted metabolomics studies. Anal. Chem. 88:8082-8090.

Tzin, V., and Galili, G. 2010. The biosynthetic pathways for shikimate and aromatic amino acids in *Arabidopsis thaliana*. Arabidopsis Book 2010: e0132.

Vargas, W. A., Djonović, S., Sukno, S. A., and Kenerley, C. M. 2008. Dimerization controls the activity of fungal elicitors that trigger systemic resistance in plants. J. Biol. Chem. 283:19804-19815.

Vaughan, M. M., Block, A., Christensen, S. A., Allen, L. H., and Schmelz, E. A. 2018. The effects of climate change associated abiotic stresses on maize phytochemical defenses. Phytochem. Rev. 17:37-49.

Vicente, I., Baroncelli, R., Morán-Diez, M. E., Bernardi, R., Puntoni, G., Hermosa, R., Monte, E., Vannacci, G., and Sarrocco, S. 2020. Combined comparative genomics and gene expression analyses provide insights into the terpene synthases inventory in *Trichoderma*. Microorganisms 8: 1603.

Vinci, G., Cozzolino, V., Mazzei, P., Monda, H., Spaccini, R., and Piccolo, A. 2018. An alternative to mineral phosphorus fertilizers: The combined effects of *Trichoderma harzianum* and compost on *Zea mays*, as revealed by ^{1}H NMR and GC-MS metabolomics. PLoS One 13:e0209664.

Von Rad, U., Hüttl, R., Lottspeich, F., Gierl, A., and Frey, M. 2001. Two glucosyltransferases are involved in detoxification of benzoxazinoids in maize. Plant J. 28:633-642. 10.1046/j.1365-313x.2001.01161.x

Walker, V., Bertrand, C., Bellvert, F., Moënne-Loccoz, Y., Bally, R., and Comte, G. 2011. Host plant secondary metabolite profiling shows a complex, strain-dependent response of maize to plant growth-promoting rhizobacteria of the genus *Azospirillum*. New Phytol. 189:494-506.

Wang, K. D., Borrego, E. J., Kenerley, C. M., and Kolomiets, M. V. 2020. Oxylipins other than jasmonic acid are xylem-resident signals regulating systemic resistance induced by *Trichoderma virens* in maize. Plant Cell 32:166-185.

Wang, X., Chen, Q., Wu, Y., Lemmon, Z. H., Xu, G., Huang, C., Liang, Y., Xu, D., Li, D., Doebley, J. F., and Tian, F. 2018. Genome-wide analysis of transcriptional variability in a large maize-teosinte population. Mol. Plant 11:443-459.

Yedidia, I., Shoresh, M., Kerem, Z., Benhamou, N., Kapulnik, Y., and Chet, I. 2003. Concomitant induction of systemic resistance to *Pseudomonas syringae* pv. *lachrymans* in cucumber by *Trichoderma asperellum* (T-203) and accumulation of phytoalexins. Appl. Environ. Microbiol. 69: 7343-7353.

Zamioudis, C., and Pieterse, C. M. 2012. Modulation of host immunity by beneficial microbes. Mol. Plant-Microbe Interact. 25:139-150.

Zeilinger, S., Gruber, S., Bansal, R., and Mukherjee, P. K. 2016. Secondary metabolism in *Trichoderma* – Chemistry meets genomics. Fungal Biol. Rev. 30:74-90.

Zhou, S., Richter, A., and Jander, G. 2018. Beyond defense: Multiple functions of benzoxazinoids in maize metabolism. Plant Cell Physiol. 59:1528-1537.